

Excitonic properties of ZnSe/(Zn,Mg)Se quantum wells: A model study of the tensile-strain situation

J. Puls, M. Rabe, A. Siarkos, and F. Henneberger

Humboldt-Universität zu Berlin, Institut für Physik, 10115 Berlin, Germany

(Received 16 December 1997)

We present a comprehensive study of the excitonic properties of ZnSe/(Zn,Mg)Se structures grown by molecular beam epitaxy. Magnetoabsorption is used to derive precise values of the exciton binding energies and reduced in-plane masses. The data demonstrate a remarkable enhancement of both quantities due to heavy-hole-light-hole coupling in the tensile strained wells, independently verified by a calculation of the hole subband dispersions and the resulting reduced exciton masses in the frame of the Luttinger Hamiltonian. The large exciton binding energies (≈ 38 meV) signify a valence band offset of about 30% of the total band offset. The increased exciton stability as well as the accordingly reduced coupling to LO phonons result in dominant exciton contributions to the photoluminescence and optical absorption up to temperatures of 240 K. At low temperatures, the localization of excitons on well thickness fluctuations, directly traced in time-resolved luminescence, gives rise to a dominant inhomogeneous broadening. A pronounced biexciton luminescence band is observed at elevated excitation densities. [S0163-1829(98)04123-X]

I. INTRODUCTION

Ternary and quaternary II-VI semiconductors containing Mg have been successfully applied as wave-guiding and cladding layers in blue laser structures.^{1,2} Both band-gap and lattice constant are increased by adding Mg to ZnSe-based compounds, allowing one to shift the operation wavelength of the diodes deeper into the blue and, in combination with S, to grow quaternary (Zn,Mg)(Se,S) layers lattice matched to the commonly used GaAs substrates, respectively. Already the ternary (Zn,Mg)Se material offers the possibility to fabricate quantum well (QW) structures for studying quasi-two-dimensional excitons in II-VI semiconductors. In comparison with the widely studied (Zn,Cd)Se/ZnSe QW's, the use of (Zn,Mg)Se barriers provides a number of interesting features. Firstly, the well can be formed by the *binary* ZnSe compound, confining alloy disorder to the barriers from which a reduced inhomogeneous broadening is expected. Secondly, the well is under tensile strain. Thus, the interplay of confinement and strain effects enables us to tune light-hole (lh) and heavy-hole (hh) exciton states into resonance by reducing the well width. The excitonic properties of ZnSe/(Zn,Mg)Se QW's are expected to be similar to the previously studied ZnSe/(Zn,Mn)Se structures^{3,4} because of the comparable strain situation. However, the use of Mg instead of Mn allows us to avoid nonradiative transitions associated with inner Mn^{2+} states and the distinct bowing of (Zn, Mn)Se at low temperatures, caused by the semimagnetic behavior of Mn^{2+} .

The formation of truly quasi-two-dimensional excitons critically depends on the confinement of both electron and hole in the well, which requires an adequate valence-band offset (VBO) at the ZnSe/(Zn,Mg)Se heterointerface. The data reported so far are very diverging. A vanishing VBO according to the "common anion rule" has been concluded from PL studies on ZnTe/(Zn,Mg)Se QW's.⁵ On the other hand, x-ray photoelectron spectroscopy has yielded a distinct

VBO for lattice-matched MgSe and (Zn,Cd)Se, which contradicts this rule.⁶ Moreover, calculations⁷ have predicted that the valence-band edge of MgSe is indeed some 100 meV below the one of ZnSe due to the absence of *d* core states for Mg. Very recently, an even larger VBO (0.87 of the total band offset) has been deduced from both optical and photoelectron spectroscopy.⁸

In this paper, we focus on the properties of excitons in ZnSe/(Zn,Mg)Se QW's grown by molecular beam epitaxy (MBE). On a set of specially grown samples, ground-state energies of the hh and lh excitons are derived in dependence on the Mg content x and the well thickness d by photoluminescence excitation spectroscopy at low temperatures. We have varied d from nearly one-half to twice of the ZnSe bulk exciton radius [$a_B = 4.5$ nm (Ref. 9)], whereas x was restricted to values below 0.3 because of the strongly increasing lattice mismatch. For a multiple QW (MQW) with intermediate x and d , we have performed magneto-optical studies to uncover excited exciton states from which very precise data on exciton binding energies and band masses can be extracted. The magneto-optical data are analyzed by extensive numerical calculations. After treating the strain-induced splitting of hh and lh bands, single-particle confinement energies and exciton binding energies are computed in a two-band model, using either a two-parameter variational ansatz for the relative motion or by fully solving the in-plane exciton Schrödinger equation. The latter ignores Coulomb correlation in the growth direction, but allows one to calculate the complete set of exciton states in a magnetic field.¹⁰ The analysis of the experimental data reveals a dramatic increase of the in-plane hole masses in comparison with the widely used diagonal approximation of the Luttinger Hamiltonian. To figure out the significance of the off-diagonal elements for the present structures, we perform additionally a calculation of the lh and hh subband dispersion and the exciton related in-plane masses, taking into account the full coupling of the Γ_8 valence band.

For the calculations, a detailed knowledge of the barrier heights and the strain in the QW's is required. Since available data^{8,11–14} on the gap energy of (Zn,Mg)Se rely mainly on room-temperature studies, we have included a characterization of the alloy material at low temperatures as well. A nearly perfect agreement between observed and calculated exciton energies is achieved, if a VBO of 30% of the total band offset for the unstrained materials is assumed. Binding energies of nearly 40 meV are derived for both the lh and hh exciton. Consistently, a dominating contribution of excitons to the QW absorption and luminescence spectra is found up to a temperature of 240 K. Our study is completed by time-resolved luminescence spectroscopy at low temperatures, indicating a leading radiative recombination and a weak localization on interface roughness. At intermediate excitation densities, a formation of lh biexcitons is observed with a binding energy of 9 meV.

II. EXPERIMENTAL RESULTS

The samples were grown on [001]-oriented GaAs substrates by MBE using a thick (0.5–1.0 μm) ZnSe buffer as well as a 1- μm -thick (Zn,Mg)Se layer. The structures themselves consist of either a single ZnSe QW capped with 85 nm (Zn,Mg)Se or five QW's separated by 85-nm (Zn,Mg)Se barriers. Employing phase-locked epitaxy,¹⁵ the reflection high-energy electron diffraction (RHEED) oscillations were utilized to control the growth via a feedback mechanism. This technique provides sharper interfaces and a precise knowledge of the QW thickness. The Mg content and lattice constants of the ternary (Zn,Mg)Se layers were determined by electron-beam microanalysis and high-resolution x-ray diffraction, respectively. Despite of the large thickness of the (Zn,Mg)Se buffer, a remarkable compressive in-plane strain of about -6×10^{-4} was found for the barriers at room temperature, indicating an uncompleted relaxation during the growth. In good approximation, the unit cell symmetry turns from a cubic into a tetragonal one. The lattice constant a of the unstrained (Zn,Mg)Se was deduced from the constants of the strained layers measured perpendicular and parallel to the growth direction. The ratio of the elasticity tensor components c_{12}/c_{11} was set equal to 0.6 according to ZnSe.⁹ In excellent agreement with Vegard's rule, the data can be linearly interpolated in the studied Mg range:

$$a(x) = (0.56688 + 0.02947x) \text{ nm}. \quad (1)$$

It should be noted that the error-free (95% statistical certainty) lattice constant extrapolated for zinc-blende MgSe $a(1) = 0.5964 \pm 0.025$ nm is distinctly larger than previously reported values.^{8,11,12}

The variation of the band-gap energy E_g with Mg admixture was derived from the barrier photoluminescence (PL) being even stronger than the one of QW excitons (see Fig. 1). According to the strain situation, the barrier PL has to be assigned to the hh exciton. The linewidth increase for growing Mg fraction reflects directly the role of alloy disorder in the (Zn,Mg)Se bulklike layers. At least partially, we attribute the more intense PL from the barrier in the single QW structures to a disorder-induced reduction of the exciton mobility. Neglecting the small strain shift (<5 meV), the band gap of the ternary alloy was deduced from the PL band assuming

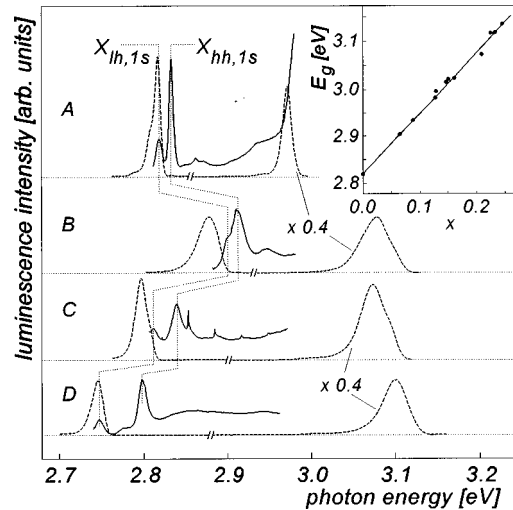


FIG. 1. PL (dashed) and PLE (solid lines) spectra of four single QW structures with A, $x=0.145$, $d=4.5$ nm; B, 0.26, 2.3 nm; C, 0.24, 4.5 nm; and D, 0.26, 9.0 nm. $T=5$ K. PL spectra are taken under UV excitation with an Ar^+ laser. Dotted lines are used to mark the ground states of lh and hh exciton in the wells. Inset: Variation of the (Zn,Mg)Se band-gap energy E_g vs x as derived from barrier PL (see text). The line represents the fit of data by Eq. (2).

the same exciton binding energy as for ZnSe [18 meV (Ref. 9)] and an alloy disorder-induced Stokes shift¹⁶ of one-half of the barrier PL bandwidth [full width at half maximum (FWHM)]. As seen in the inset of Fig. 1, the data obtained at 5 K can be well fitted by a linear relation:

$$E_g = (2.82 + 1.28x) \text{ eV}. \quad (2)$$

No hint of a bowing in the $E_g(x)$ relation is found in the limited Mg range studied ($x < 0.3$).

While the (Zn,Mg)Se layers show a weak compressive deformation, the QW's are under strong tensile strain. Accordingly, the low-energy PL bands in Fig. 1 have to be attributed to the lh exciton. This was confirmed by PL excitation (PLE) spectroscopy, by which the ground states of both the lh ($X_{lh,1s}$) and the hh excitons ($X_{hh,1s}$) were clearly identified. The intensity ratio between the lines is close to the expected 1:3 rule. The confinement-induced shift of the exciton states, displayed in Fig. 1 for the samples B–D with practically the same x but different well thicknesses, is more pronounced for $X_{lh,1s}$ due to the lighter hole mass along growth direction. This behavior results in a decrease of lh-hh splitting with decreasing d . At the same time, the QW exciton features become broader and the Stokes shift between PL and PLE increases. We conclude that interface roughness gives a remarkable contribution to the inhomogeneous width of the exciton lines. This result is not in conflict with the improved interface quality achieved by the phase-locked epitaxy modus. The disorder-induced broadening scales as the product of island area and height,¹⁷ so that a smoothing of the interface does not necessarily result in sharper PL lines. For sample C, spectrally narrow phonon replica are seen in PLE. We assign these features to Raman scattering from the thick ZnSe buffer, since the detection wavelength is here occasionally very close to the ZnSe bulk exciton ground state.

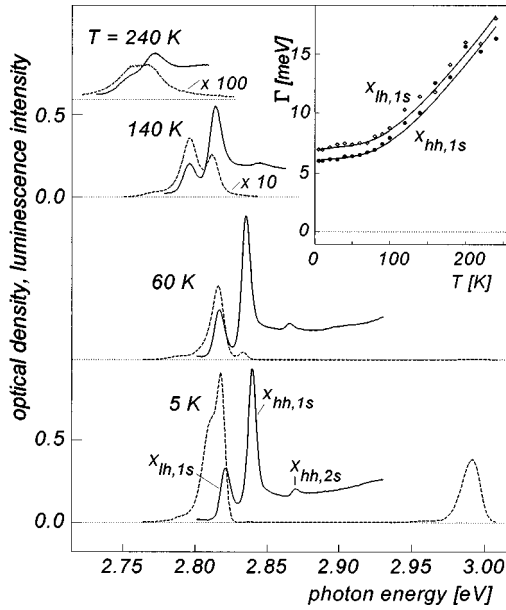


FIG. 2. PL (dashed) and absorption (solid lines) spectra of a MQW structure for various temperatures ($x=0.15$, $d=4.5$ nm). Inset: Width (FWHM) of $X_{hh,1s}$ (solid) and $X_{lh,1s}$ (open circles) absorption line vs temperature. Lines are fits of the temperature dependence with Eq. (3).

Increasing the energy barrier via the Mg content, the expected high-energy shift of the QW exciton states is overcompensated by strain effects. As seen by the samples A and C, a change of x from 0.145 to 0.24 at fixed $d=4.5$ nm causes even a low-energy shift of $X_{lh,1s}$ and increases the hh-lh splitting. For the samples B to D, no higher subband transitions are found in the PLE spectra that may be caused by the limited spectral range provided by the Stilben 3 dye laser. For sample A with smaller barrier height, the PLE spectrum could be measured up to the steep rise around 2.97 eV, marking the onset of barrier excitation. As for the other samples, no sharp structures displaying the existence of higher subband transitions are seen.

From the clear exciton resonances observed in PLE at 5 K, the question arises about their contribution at elevated temperatures. We have thus studied the temperature dependence of PL and absorption on a MQW structure. For the latter, the transmission was measured on a sample piece, where the substrate and the ZnSe buffer had been removed by selective wet etching. The data were corrected for Fabry-Pérot effects. In Fig. 2, absorption and PL spectra at selected temperatures are depicted. In the absorption spectrum at 5 K, pronounced lines of the lh and hh 1s ground-state excitons are again seen with a linewidth Γ (FWHM) of less than 6 meV (hh) and 7 meV (lh), respectively. The ratio between the oscillator strengths (spectrally integrated absorption) of $X_{hh,1s}$ and $X_{lh,1s}$ amounts to 2.7 ± 0.3 . With growing temperature, an increasing broadening occurs. Nevertheless, the exciton lines are clearly visible up to temperatures above 200 K. The inset of Fig. 2 represents the temperature dependence of Γ for both exciton lines, deduced from a fit of the absorption spectra with two Lorentzian-like exciton lines and a broadened steplike function, the latter representing the lh subband edge located energetically slightly above $X_{hh,1s}$. The lines are calculations using the standard formula

$$\Gamma(T) = \Gamma_0 + \Gamma_{ac}T + \frac{\Gamma_{LO}}{\exp(\hbar\omega_{LO}/k_B T) - 1}, \quad (3)$$

where Γ_{ac} and Γ_{LO} denote the coupling strength of excitons to acoustic and longitudinal optical phonons, respectively. For the LO-phonon energy $\hbar\omega_{LO}$, we used the well-known value of ZnSe [31.5 meV (Ref. 9)]. A slightly higher inhomogeneous part Γ_0 found for $X_{lh,1s}$ is at least qualitatively expected, since the lh exciton energy is more sensitive on well thickness fluctuations. However, both exciton transitions undergo practically the same broadening with increasing temperature. The parameters derived by the fit are given in Table II at the end of the next section. The temperature-induced broadening of exciton lines in PL exhibits a similar trend. At 5 K, the pronounced $X_{lh,1s}$ PL band is accompanied by a weaker bound exciton transition, indicated by a low-energy shoulder. As for the single QW structures in Fig. 1, the PL from the barrier around 2.99 eV yields a contribution comparable to the QW luminescence. Already at 60 K, the barrier PL drops drastically down, indicating the increased mobility of barrier excitons at higher temperatures. In the QW region, the bound exciton transition disappears, while a more and more intense $X_{lh,1s}$ PL reflects the growing thermal occupation of this state. Although an overall thermal quenching of the luminescence clearly occurs, it should be emphasized that QW excitons but not free carrier transitions are dominant even at 240 K. An Arrhenius plot of the spectrally integrated QW PL demonstrates that the PL quenching is not controlled by a single activation energy. For higher temperatures ($T > 100$ K), we estimate an activation energy of about 50 meV.

In some of the PLE spectra (see Fig. 1) as well as in the low-temperature absorption spectra, weak structures roughly 30–40 meV energetically above the respective exciton ground states indicate the energy positions of excited exciton states or the subband edge, respectively. Magneto-optics is known to be a powerful tool to study such features in more detail and to derive precise values of the exciton binding energies and band masses. Magnetoabsorption studies on the present structures were carried out using a 12 T-OXFORD split coil magnet in Faraday geometry (field B along growth direction). In this way, we were able to uncover magnetoexcitons up to the 3s and 5s level of the lh and hh exciton, respectively. The energies of magnetoexcitons are drawn in Fig. 3 versus B for both orientations of the circularly polarized light. The lines represent calculated magnetoexciton energies (see next section). The splitting between the σ^+ and σ^- active states reflects simply the standard Zeeman effect with two exceptions: $X_{hh,1s}$ shows an unusual large splitting, whereas the splitting of $X_{lh,2s}$ is reversed. We have fitted the magnetic field behavior of both ground-state excitons by a sum of a zero-field energy E_0 , a Zeeman splitting $\pm g_{eff}\mu_B B$ (μ_B is the Bohr magneton) and a diamagnetic shift δB^2 , the result of which is also given in Table II.

Time-resolved and intensity-dependent PL measurements at low temperatures were carried out exciting the MQW structure resonantly at the $X_{hh,1s}$ transition by the output train of a mode-locked dye laser synchronously pumped by the third harmonic of a Nd:YLF (yttrium lithium fluoride) laser. The pulse duration was 2 ps at 76-MHz repetition rate, yielding exciton densities up to some 10^{11} cm $^{-2}$. Time-integrated

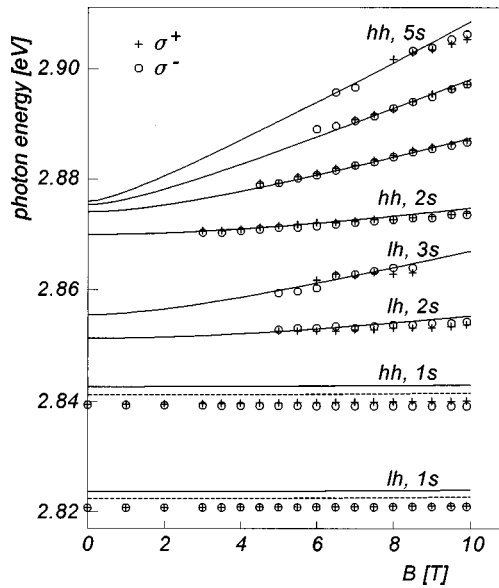


FIG. 3. Circles and crosses: energies of magnetoexcitons observed in absorption for σ^+ and σ^- polarized light, respectively, vs B . Sample as in Fig. 2. $T=1.8$ K. Lines: calculated energies of magnetoexcitons (see Sec. III).

spectra recorded by an OMA system are given in Fig. 4 for different excitation fluxes Φ . For the lowest Φ applied, the photoexcited carrier density is more than one order of magnitude higher than for the PL spectra in Fig. 2. Consistently, the bound exciton contributions on the low-energy side of $X_{lh,1s}$ are already saturated. A further increase of excitation density yields a sublinear growth of the exciton emission band and the appearance of a new band (XX), which becomes dominant at the highest Φ . The overall picture is very similar to observations on (Zn,Cd)Se/ZnSe wells, where a

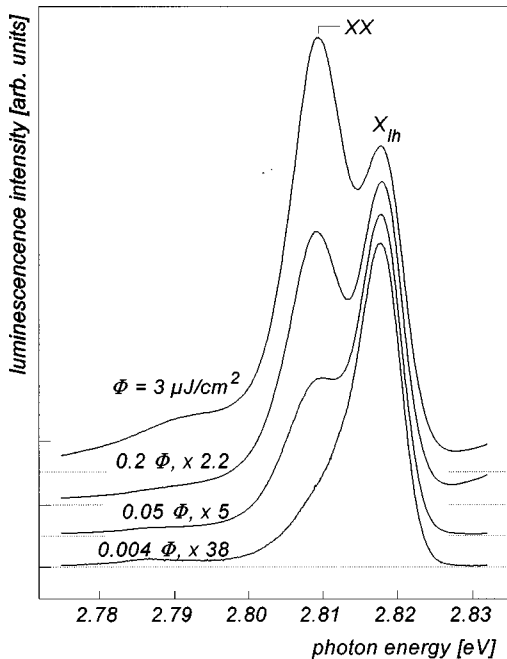


FIG. 4. Time-integrated PL spectra using pulsed ps-excitation resonantly to $X_{lh,1s}$ at various excitation levels. Sample as in Fig. 2. $T=5$ K.

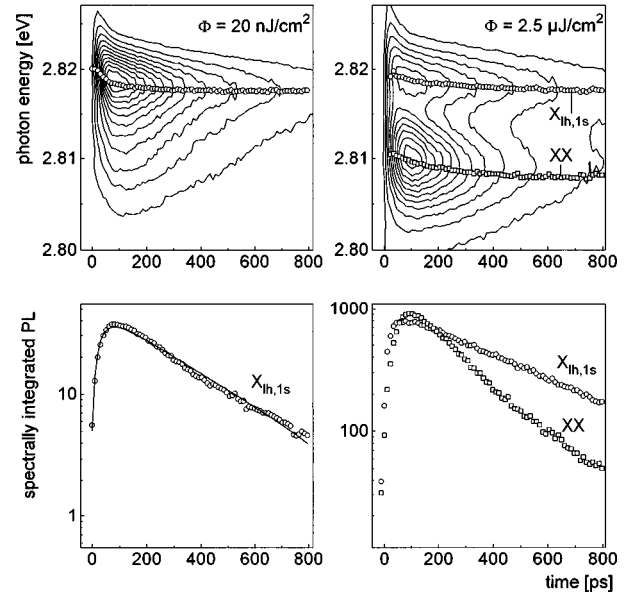


FIG. 5. Upper part: Contour map of the time-resolved PL at low and high excitation fluxes Φ . Open circles and squares are used to mark the maximum position of the $X_{lh,1s}$ and XX band, respectively. Lower part: Spectrally integrated intensity of the $X_{lh,1s}$ and XX bands vs delay time. Assignment of symbols and excitation fluxes as in the upper part. The line in the lower left part represents a fit of the $X_{lh,1s}$ transient (see text). Sample as in Fig. 2. $T=5$ K.

biexcitonic luminescence emerges below the lowest exciton ground state at comparable densities (see Ref. 18 and papers cited therein). Following previous work,¹⁸ we have confirmed the biexcitonic nature of the XX band observed here by applying a magnetic field in Faraday geometry. The XX band did not show any polarization as being characteristic of biexciton recombination. Unlike (Zn,Cd)Se/ZnSe QW's, the biexciton in the ZnSe/(Zn,Mg)Se structures is composed of two lh excitons as a result of the tensile in-plane strain. A binding energy of 9 meV is derived from the energy spacing between the $X_{lh,1s}$ and the XX band.

For time-resolved measurements, the PL was spectrally decomposed by a double monochromator in a subtractive dispersion mode and recorded by a synchroscan streak camera, enabling an overall time and spectral resolution of 10 ps and 0.5 meV, respectively. Time-resolved spectra were constructed from the PL decay traces taken at a sufficient number of points across the relevant spectral range. In the upper part of Fig. 5, the respective spectra are given by contour plots for low and high excitation fluxes. At low flux, only the $X_{lh,1s}$ PL band appears, which undergoes a clearly resolved low-energy shift during the first 150 ps. As seen by the open circles marking the maximum position of the PL band, the total shift caused by the increasing localization amounts to 2 meV. The lower left part of Fig. 5 depicts the transient behavior of the spectrally integrated PL. Deconvolution of this curve with the simultaneously registered excitation pulse yields a rise and decay time of $\tau_r=35$ ps and $\tau_{lh}=310$ ps, respectively. It should be noted that first the decay time increases with growing sample temperature (450 ps at 40 K), while a shortening of the decay sets in above 60 K.

To derive the maximum positions and the spectrally integrated PL of the $X_{lh,1s}$ and XX band as a function of delay

TABLE I. Parameters of ZnSe used in the calculations.

a_H (eV)	b_S (eV)	Δ_{so} (eV)	c_{12}/c_{11}	m_e/m_0	γ_1	γ_2	γ_3	ε_0
-4.25 ^a	-1.2 ^a	0.43 ^b	0.6 ^b	0.147 ^c	2.45 ^c	0.61 ^c	1.11 ^c	8.8 ^b

^aReference 24.^bReference 9.^cReference 25.

time for high excitation levels, we decomposed the time-resolved spectra in two bands. As seen in the upper right hand side part of Fig. 5, both bands show a transient low-energy shift again. Whereas the total shifts are quite similar to that of $X_{lh,1s}$ at low densities, the localization process of excitons and biexcitons is now distinctly slower. We attribute this to an increased filling and saturation of localization sites, established at photoexcited exciton densities of some 10^{11} cm^{-2} . The maximum of the spectrally integrated XX PL occurs more than 100 ps delayed with respect to the excitation pulse and the decay has a time constant of $\tau_{XX} = 200$ ps. Simultaneously, a slowing down of the $X_{lh,1s}$ decay is observed. This is related to the creation of single excitons by the radiative recombination of biexcitons.

III. CALCULATION OF EXCITON ENERGIES

To deduce the relevant exciton and band parameters of this type of QW structure, we compare the exciton energies found in PLE and magneto-optical studies with calculated values in this chapter. After considering the band discontinuities, the calculation of confinement energies and exciton binding energies follows quite closely routines previously successfully applied for magnetoexcitons in (Zn,Cd)Se/ZnSe QW's.¹⁹ Hence, we focus here on the discussion of the offset problem and the reader is referred for more details to Ref. 19. We recall that this calculation relies on a two-band model applied separately to the hh and lh exciton series. Because of the decreased splitting between those states in thinner QW's, this seems to be somewhat questionable in this case. However, a full treatment of magnetoexcitons on the basis of the Luttinger Hamiltonian is beyond the scope of this paper. To account for the lh-hh coupling at least in lowest order, the reduced in-plane exciton mass μ_p is used as a fit parameter in the two-band approximation.²⁰ To check the reliability of the masses derived this way, we present a calculation of the hole subband dispersions and exciton envelope functions at $B=0$ based on the Luttinger model²¹ at the end of this chapter.

Assuming the well width below the critical thickness of ZnSe on (Zn,Mg)Se, i.e., pseudomorphically grown QW's, the in-plane strain ε at room temperature can be precisely derived from the lattice constant of unstrained ZnSe and the measured in-plane constant of the (Zn,Mg)Se layer. The strain alteration between room temperature and 5 K is neglected. The conduction, hh and lh valence-band edges in the tensile strained ($\varepsilon > 0$) ZnSe well are given by²²

$$E_c = E_g(0) + \delta E_{H,c}, \quad (4)$$

$$E_{hh} = -\delta E_{H,v} + \delta E_S, \quad (5)$$

$$E_{lh} = -\delta E_{H,v} - \delta E_S - \frac{1}{2}[\Delta_{so} - \delta E_S - \sqrt{(\Delta_{so} - \delta E_S)^2 + 8(\delta E_S)^2}] \quad (6)$$

with the hydrostatic strain-induced energy shift of the conduction and valence band

$$\delta E_{H,i} = 2a_{H,i}(1 - c_{12}/c_{11})\varepsilon, \quad i = c, v \quad (7)$$

and the one induced by uniaxial strain

$$\delta E_S = b_S(1 + 2c_{12}/c_{11})\varepsilon. \quad (8)$$

$a_H = a_{H,c} + a_{H,v}$ and b_S are the hydrostatic and uniaxial deformation potentials, respectively. Δ_{so} is the spin-orbit splitting. All energies are measured relative to the top of the valence band of unstrained ZnSe. Little is known about how the total hydrostatic strain potential is shared between the conduction and valence band. In the following, we use an intermediate value $a_{H,v} = 0.3a_H$ successfully applied to calculate exciton energies in (Zn,Cd)Se/ZnSe QW's.²³ The band-edge energies in the barrier layers are obtained by assigning the Mg-induced gap shift (2) by $(1 - Q_v)$ and Q_v to the conduction and valence band, respectively, where Q_v denotes the ratio between the VBO and the total band offset. We note that both $a_{H,v}$ and Q_v determine the actual hh and lh valence-band offset in the presence of strain. Therefore, the values of these two parameters cannot be determined independently here. The small splitting between hh and lh bands (< 5 meV) due to the residual strain in the barrier has been neglected in the calculations. The total energies of lh and hh excitons can be expressed by

$$E_{ex,h} = E_c - E_h + E_{qc,e} + E_{qc,h} - E_{ex,h}^b \quad (h = lh, hh), \quad (9)$$

where $E_{qc,e}, E_{qc,h}$ are the confinement energies of electron and hole, respectively. $E_{ex,h}^b$ denotes the exciton binding energy. For the exciton wave function, the separation ansatz

$$\Psi(\rho, z_e, z_h) = \frac{1}{\sqrt{2\pi}} \phi(\rho) \varphi_e(z_e) \varphi_h(z_h) \quad (10)$$

is used, considering only optically active exciton states with s -like symmetry at zero center-of-mass momentum. $\varphi_{e,h}$ denote the electron and hole subband wave functions, respectively. For treating the magnetoexciton states, the remaining one-dimensional Schrödinger equation for $\phi(\rho)$ is solved by the finite difference method.¹⁰ The material parameters used

TABLE II. Deduced exciton parameters of the ZnSe/(Zn,Mg)Se MQW in Fig. 2.

	E_g^* (eV)	$\mu_{p,h}/m_0$	$E_{ex,h}^b$ (meV)	g_{eff}	δ ($\mu\text{eV}/T^2$)	Γ_0 (meV)	Γ_{ac} ($\mu\text{eV}/K$)	Γ_{LO} (meV)
X_{lh}	2.858	0.135	37.8	0.139	3.16	6.94	6.7	34.7
X_{hh}	2.877	0.125	37.6	(0.848)	(2.22)	6.00	6.7	35.0

are summarized in Table I. The hole masses along the growth direction ($m_{hh}=0.813m_0$, $m_{lh}=0.272m_0$) are derived from the Luttinger parameters γ_1 and γ_2 , using the diagonal approximation of the Luttinger Hamiltonian. Since precise values of the carrier masses are not available for the (Zn,Mg)Se alloy, we adopted the ZnSe values for the barrier too.

As pointed out in Ref. 19, both the reduced in-plane exciton mass $\mu_{p,h}$ and the energy gap between the lowest subbands $E_{g,h}^*=E_{ex,h}+E_{ex,h}^b$ can be very precisely derived from a fit of the *excited* magnetoexciton states. The band offsets are much less important. Therefore, we start the calculations assuming an intermediate Q_v of 0.3. The enumerated magnetoexciton energies are given by solid lines in Fig. 3. As seen, a very satisfactory fit of the magnetic-field dependence of excited lh and hh states is achieved. The resulting subband gaps and reduced in-plane masses are summarized for both the lh and hh series in Table II. For the ground-state excitons, the agreement between the experimental data and the calculations is less perfect. This is, at least partly, caused by the neglect of Coulomb correlation along growth direction in the ansatz (10). Nevertheless, the desired exciton binding energies can be very accurately deduced from the difference of the respective subband gap energy, known from the excited-state fit and the experimental photon energy of the exciton ground state at $B=0$. The respective values are included in Table II. To account for the Coulomb correlation along growth axis, we have performed additionally a variational treatment of the ground states using a two-parameter trial function (TPVT; two-parameter variational treatment)

$$\phi(\rho, z_e - z_h) = N^{-1/2} \exp \left[-\frac{1}{a} \sqrt{\rho^2 + \beta^2 (z_e - z_h)^2} \right] \quad (11)$$

instead of $\phi(\rho)$ in Eq. (10). The parameter a is the Bohr radius and β accounts for the dimensionality of the exciton. Both parameters are determined by minimizing the respective exciton energy. Within first-order perturbation theory, the diamagnetic shift can be computed from the wave function (11). The results of the TPVT are given by dashed lines in Fig. 3. In the calculation, the reduced in-plane masses derived above have been used. Indeed, the inclusion of the electron-hole correlation along growth direction increases the binding energies by about 2 meV and yields a better description of the experimental data. Since the diamagnetic shifts of the exciton ground states are hardly seen in Fig. 3 due to the enlarged energy scale, we note that the calculations reproduce the $X_{lh,1s}$ magnetic field behavior quite well. For $X_{hh,1s}$, however, the experimental value of δ is about 50% smaller than the one calculated in the two-band model.

Up to this point, an intermediate value of the valence-band offset has been assumed in the calculations. In the following, we study the dependence of $E_{ex,h}^b$ on the VBO using now the variational treatment. To do this, one should keep in mind that a reduction of the VBO results at a certain value in a ‘‘type 1’’ to ‘‘type 2’’ transition in the band alignment. According to the strain situation, this appears at first for the hh band. In this case, the TPVT described above is no longer applicable. To cover this range of VBO too, we have alternatively applied a modified variational treatment, where the hole subband wave function is self-consistently calculated from the resulting potential of the band offset and the Coulomb attraction caused by the confined electron. Details on this procedure are given in Ref. 26. For simplification, only a in Eq. (11) is varied during the minimization of the exciton energy, whereas the parameter β is set to 1. That corresponds to a three-dimensional exciton trial function, being surely appropriate for a valence-band offset around zero. We refer to this treatment in the following by VTSCWF (variational treatment with self-consistent hole wave function). In Fig. 6, we have plotted QW exciton binding energies calculated by TPVT and VTSCWF versus Q_v for the well thickness and Mg fraction of the sample in Fig. 2. Note that the Q_v value refers to the unstrained situation according to the above given definition of energies in well and barrier. As seen in the case of $X_{hh,1s}$, the VTSCWF yields larger binding energies at smaller Q_v , whereas the increased confinement at higher VBO yields a transition to a rather two-dimensional exciton, more adequately described by the TPVT. A comparison with the experimental binding energies, marked by arrows on the left-hand axis, directly proves that a VBO of more than 20% of the total band offset is required to explain the experimental binding energies of $X_{lh,1s}$ and $X_{hh,1s}$ as well

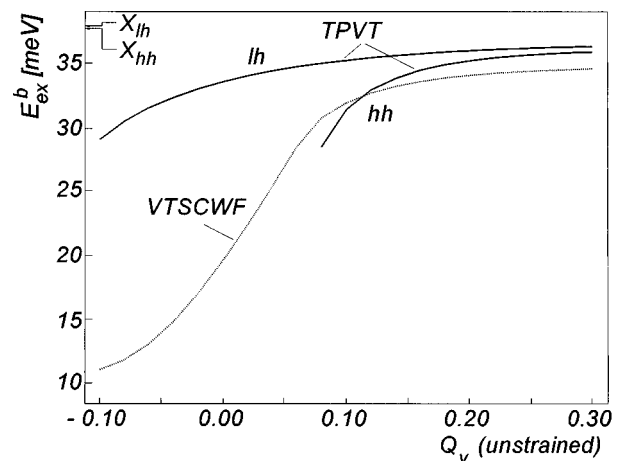


FIG. 6. Calculated hh and lh exciton binding energies vs the relative valence-band offset Q_v . x and d as for the sample in Fig. 2. Since the considered range of VBO ensures large enough offset in the lh band, only the results of the TPVT are given for this exciton.

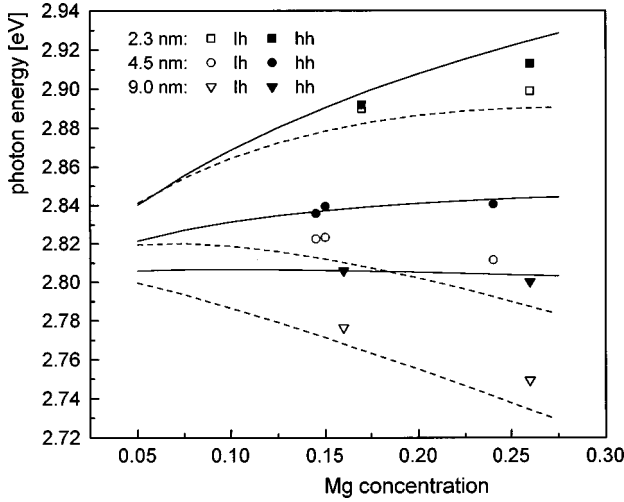


FIG. 7. Comparison between experimental $X_{hh,1s}$ and $X_{lh,1s}$ photon energies (PLE) given by solid and open symbols and calculated ones given by solid and dashed lines, respectively, for three QW thicknesses.

as that their values are very close to each other. Using the intermediate $Q_v = 0.3$ and adding the strain contribution, a total valence-band offset of 84 and 44 meV in the lh and hh band, respectively, follows for a Mg fraction of 0.15. An increase of Q_v above 0.6 (not drawn in Fig. 6) again diminishes the lh and hh exciton binding energies due to a decreasing electron confinement. In this case, the values are remarkable below the experimental ones, defining thus an upper limit for this parameter.

Finally, we applied the TPVT to calculate the exciton energies of $X_{lh,1s}$ and $X_{hh,1s}$ for the set of QW's studied experimentally. Again, the ZnSe parameter in Table I and the reduced in-plane masses derived by the fit of excited magnetoexcitons as well as $Q_v = 0.3$ were used. In Fig. 7, the total exciton energies are drawn versus Mg concentration for the relevant well thicknesses and compared with the experimental values. A quite satisfactory description of the experimental data set is again achieved. The small deviations found for the lh excitons seems to be systematic. Probably, they are caused by a reduction of the tensile strain during cooling of the samples from room temperature to 5 K. A variation of Q_v between 0.2 to 0.6 yields practically the same data for $d = 4.5$ and 9.0 nm. A dependence of the total exciton energies on Q_v obtained for 2.3 nm is too weak to restrict further the possible range of the VBO.

The deduced relative in-plane masses (see Table II) deviate remarkably from those obtained by the diagonal approximation of the Luttinger Hamiltonian: $\mu_{p,hh}/m_0 = (m_0/m_e + \gamma_1 + \gamma_2)^{-1} = 0.101$ and $\mu_{p,lh}/m_0 = (m_0/m_e + \gamma_1 - \gamma_2)^{-1} = 0.116$. A similar effect has been recently reported for magnetoexcitons in CdTe/(Cd,Zn)Te QW's.²⁰ The present values are very close to the electron mass, pointing at extremely large in-plane hole masses. Going beyond the two-band model, we prove this by a calculation of the hole subbands and the respective exciton envelope functions at $B = 0$ in the frame of the Luttinger model (coupled Γ_8 valence band) in axial approximation [$\mu = 1/2(\gamma_2 - \gamma_3) = 0$]. Assuming a parabolic conduction band, the exciton wave function in momentum space is expanded in the product basis set of the

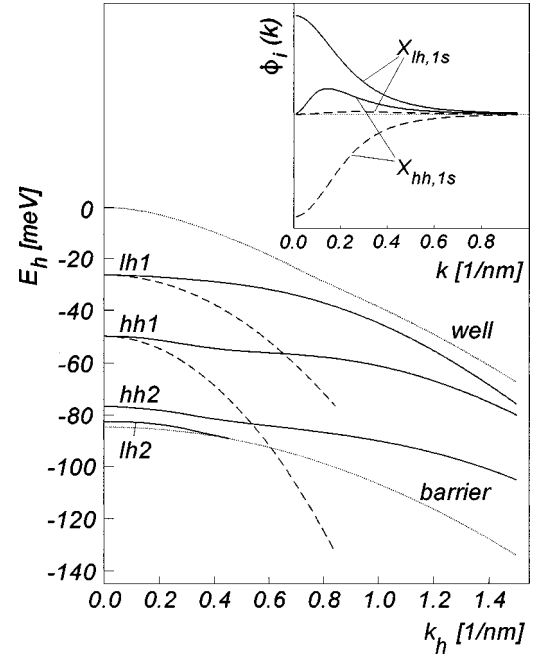


FIG. 8. Solid lines: Calculated dispersions of the lh and hh subbands in the QW structure in Fig. 2. For comparison, the results of the diagonal approximation of the Luttinger Hamiltonian are given by dashed lines. Dotted lines: Bulk valence-band edges of the well and barrier. For simplicity, the energy of the top of the well is set to zero here. Inset: Components of the Fourier-transformed $X_{lh,1s}$ and $X_{hh,1s}$ exciton envelopes for $n_h = lh1$ (solid) and $hh1$ (dashed) lines. Higher subbands do not contribute significantly.

hole and electron single-particle states for various subbands with the respective indices n_e and n_h , replacing Eq. (10) by

$$\Psi(\boldsymbol{\rho}, z_e, z_h) = \sum_{n_e, n_h} \int d\mathbf{k} \phi_{n_e, n_h}(\mathbf{k}) \varphi_{n_e}(z_e) \varphi_{n_h, \mathbf{k}}(z_h) e^{i\mathbf{k} \cdot \boldsymbol{\rho}}. \quad (12)$$

The hole-subband wave functions obtained from the Luttinger Hamiltonian depend now on the in-plane wave vector of the relative electron-hole motion $\mathbf{k} = \mathbf{k}_e = -\mathbf{k}_h$. The excitonic eigenvalue problem is solved in the basis set numerically.^{21,27} In Fig. 8, the dispersions of the lh and hh subbands of the QW structures in Fig. 3 are given by solid lines. For comparison, the results of the diagonal approximation are depicted for $n_h = lh1$ and $hh1$ by dashed ones. The deviation between both treatments is quite obvious and the decreased curvature of the calculated dispersions at the Γ point already signifies a drastic increase of the in-plane hole masses around $\mathbf{k}_h = 0$. However, the question arises of how to choose an effective value for $\mu_{p,h}$ of the two-band model appropriately. As displayed in the inset of Fig. 8, the components of the Fourier transform of the exciton envelopes spread out in the k space and, more pronounced for $X_{hh,1s}$, an admixing of lh1 and hh1 subbands takes place in both exciton ground states. A reasonable way is, hence, to require that the kinetic contribution to the exciton binding energy at $B = 0$ is reproduced correctly, which leads to the following expression for the relative exciton in-plane mass:

$$\mu_{p,h} = \frac{\hbar^2}{2m_0} \frac{\sum_{n_e, n_h} \int d\mathbf{k} \phi_{n_e n_h}^2(\mathbf{k}) k^2}{\sum_{n_e, n_h} \int d\mathbf{k} \phi_{n_e n_h}^2(\mathbf{k}) \{E_{n_e}(\mathbf{k}) + E_{n_h}(\mathbf{k}) - E_{n_e}(0) - E_{n_h}(0)\}}. \quad (13)$$

The computed values and the related in-plane hole masses $m_{p,h}$ are summarized in Table III for the lowest s -like lh exciton states and the hh exciton ground state. The exciton in-plane masses derived from the fit of the magneto-optical data in Fig. 3 compare favorably with the calculated ones. We note that the respective hole masses deviate only marginally from those following from the curvature of the hole dispersions at the Γ point. The weighted averaging (13) results in slightly smaller values for the lh exciton states because the lh1 subband at larger k follows rather closely the ZnSe bulk valence-band edge with the respective strain. The avoided crossing between the hh1 subband and higher ones, on the other hand, yields a larger $\mu_{p,h}$ value for the $X_{hh,1s}$ state. Additionally, the binding energies of both exciton series calculated within this model are given in Table III. The values remain somewhat smaller than the results of the TPVT pointing at a slight overestimation of the Coulomb attraction in the two-band model caused by the neglect of subband mixing.

IV. DISCUSSION AND CONCLUSIONS

We have successfully grown high-quality ZnSe QW's embedded between (Zn,Mg)Se barriers by MBE. The QW structures exhibit pronounced hh and lh exciton ground-state transitions. Due to the tensile in-plane strain, the lh exciton is the one of lower energy for well widths larger than 2.3 nm. The exciton energies of the QW set studied experimentally are well reproduced by a calculation within a two-band model using standard ZnSe parameters (see Table I) and, related to the unstrained case, a VBO of 0.3 of the total band offset. The fit of magneto-optical data uncovered a remarkable enlargement of the reduced exciton in-plane masses. As verified by a calculation of the hole subband dispersions, the large $\mu_{p,h}$ values arise from the enhanced heavy-hole–light-hole coupling in the tensile strained wells. In compressive strained (Zn,Cd)Se/ZnSe QW's, where the hh and lh exciton series are clearly separated by the combined action of strain and confinement, such effects are less pronounced.²⁸ On the other hand, an increased lh-hh coupling offers the possibility of “tailoring” transition energies *as well as* band masses in a desired way. Indications of an enhanced lh-hh coupling in

the present structures are also found in the magnetic-field behavior of $X_{hh,1s}$, where the parameters g_{eff} and δ obviously differ from those expected for an isolated exciton resonance. As seen in the inset of Fig. 8, a noticeable admixture of the lh1 subband with a d -like envelope occurs for $X_{hh,1s}$, resulting in a modified magnetic field behavior.²⁹ The description of the B dependence by a simple sum of Zeeman splitting and diamagnetic shift is somewhat artificial in this case and we have given therefore the respective data in parentheses in Table II.

Both the sufficiently large VBO and the enhanced in-plane mass increase the exciton stability. Already in an intermediate confinement regime ($x=0.15$, $d=4.5$ nm), the binding energy for both the lh and hh exciton is found to be twice as large as in bulk ZnSe. The experimentally observed reduction of the coupling with LO phonons— Γ_{LO} is roughly a factor of 2 smaller than for bulk ZnSe (Refs. 30 and 31)—results in clear exciton features up to 240 K. When the exciton binding energy exceeds $\hbar\omega_{\text{LO}}$, a situation applying both to the lh and hh state, a decrease of Γ_{LO} is generally anticipated, since the dissociation of the exciton by the absorption of a single LO phonon is strongly inhibited. In the present structures, however, we are faced with overlapping series of the lh and the hh exciton, which needs a reformulation of this criterion. A recent study on ZnSe/(Zn,Mg)(Se, S) QW's has yielded that the LO-phonon coupling is practically not altered in comparison with bulk ZnSe.³² This is not in conflict with our data, since the incorporation of S decreases the conduction-band offset down to 10% of the total band discontinuity,³³ by which the exciton binding energy is decreased.

The time constant of the lh exciton PL decay at low temperatures is about three times larger than in ZnSe/(Zn, Mn)Se QW structures.⁴ Although a detailed analysis has to take into account dipole-inactive excitons,²⁸ the slower decay proves nevertheless that replacing of Mn by Mg indeed suppresses nonradiative channels. The increase of τ_{lh} with growing temperature indicates a dominant radiative recombination. Compared to (Zn,Cd)Se/ZnSe QW's,³⁴ the onset of a decay shortening and the related decrease of the time-integrated PL intensity occur at lower temperatures. We believe that the moderate quenching of PL observed below 100 K is mainly caused by an increased mobility of the QW excitons, allowing them to reach nonradiative centers. The dislocation density in the present structures is enlarged by the larger lattice mismatch between the GaAs substrate and the (Zn,Mg)Se layers. The more pronounced PL quenching at higher temperatures, however, is related to the dissociation of excitons into free carriers. The activation energy found above 100 K is very close to the exciton binding energy.

The transient low-energy shift of the $X_{lh,1s}$ PL in Fig. 5 directly reflects the increasing localization of excitons on

TABLE III. Reduced exciton masses, hole masses, and exciton binding energies calculated within the Luttinger Hamiltonian.

	$\mu_{p,h}/m_0$	$m_{p,h}/m_0$	$E_{\text{ex},h}^b$ (meV)
$X_{lh,1s}$	0.138	2.22	33.1
$X_{lh,2s}$	0.138	2.20	7
$X_{lh,3s}$	0.137	2.12	3
$X_{hh,1s}$	0.133	1.38	31.3

well-width fluctuations. The total shift of 2 meV remains somewhat smaller than the Stokes shift between PL and PLE under cw excitation. Very recent micro-PL studies³⁵ have yielded markedly smaller widths of the exciton features. We conclude that about 30% of the line broadening in the present measurements stems from the experimental average over strain fields around dislocations, caused by the large excitation spot. The residual broadening seen in micro-PL is consistent with the fluctuation of 1 ML.

Characteristic for wide-gap II-VI quantum structures, an emission due to biexcitons is observed at elevated excitation intensities. Although it is formed by lh excitons, both the

binding energy and decay time are very similar to findings on hh biexcitons in (Zn,Cd)Se/ZnSe QW's.¹⁸

ACKNOWLEDGMENTS

The authors thank N. Hoffmann for a part of the sample growth, P. Schäfer for the x-ray characterization, R. Mitdank for the electron-beam microanalysis, and F. Kreller for assistance in the optical studies. R. Zimmermann and V. V. Rossin are acknowledged for helpful discussions and for providing computer programs to calculate exciton energies. One of us (A.S.) thanks E. Runge for helpful discussions. This work was supported by the Volkswagen-Stiftung within the "Photonik" program.

- ¹J. M. Gaines, R. R. Drenten, K. W. Haberern, T. Marshall, P. Mensz, and J. Petruzello, *Appl. Phys. Lett.* **62**, 2462 (1993).
- ²S. Itoh, H. Okuyama, S. Matsumoto, N. Nakayama, T. Ohata, T. Miyajima, A. Ishibashi, and K. Akimoto, *Electron. Lett.* **29**, 766 (1993).
- ³L. A. Kolodziejski, R. L. Gunshor, N. Otsuk, S. Datta, W. M. Becker, and A. V. Nurmikko, *IEEE J. Quantum Electron.* **32**, 1666 (1986).
- ⁴U. Streller, N. Hoffmann, A. Schülzgen, J. Griesche, H. Babucke, F. Henneberger, and K. Jakobs, *Semicond. Sci. Technol.* **10**, 201 (1995).
- ⁵S. O. Ferreira, H. Sitter, W. Faschinger, R. Krump, and G. Brunthaler, *J. Cryst. Growth* **146**, 418 (1995).
- ⁶M. W. Wang, J. F. Swenberg, M. C. Phillips, E. T. Yu, J. O. McCaldin, R. W. Grant, and T. C. McGill, *Appl. Phys. Lett.* **64**, 3455 (1994).
- ⁷D. J. Chadi, *Phys. Rev. Lett.* **72**, 534 (1994).
- ⁸M. Würz, E. Griebel, Th. Reisinger, R. Flierl, B. Haserer, T. Semmler, T. Frey, and W. Gebhardt, *Phys. Status Solidi B* **202**, 805 (1997).
- ⁹H. E. Gumlich, D. Theis, and D. Tschierse, in *Physics of II-VI and I-VII Compounds*, edited by O. Madelung, Landolt-Börnstein, New Series, Group III, Vol. 17, Pt. b (Springer, Berlin, 1987).
- ¹⁰J. Engbring and R. Zimmermann, *Phys. Status Solidi B* **172**, 733 (1992).
- ¹¹H. Okuyama, K. Nakano, T. Miyajima, and K. Akimoto, *Jpn. J. Appl. Phys., Part 2* **30**, L1620 (1991).
- ¹²M. Th. Litz, K. Watanabe, M. Korn, H. Röss, U. Lunz, W. Ossau, A. Waag, G. Landwehr, Th. Walter, B. Neubauer, D. Gerthsen, and U. Schüssler, *J. Cryst. Growth* **159**, 54 (1996).
- ¹³B. Jobst, D. Hommel, U. Lunz, T. Gerhard, and G. Landwehr, *Appl. Phys. Lett.* **69**, 97 (1996).
- ¹⁴E. Griebel, B. Haserer, T. Frey, T. Reisinger, and W. Gebhardt, *Phys. Status Solidi B* **198**, 355 (1996).
- ¹⁵J. Griesche, N. Hoffmann, and K. Jacobs, *J. Cryst. Growth* **138**, 59 (1994).
- ¹⁶S. Permogorov and A. Reznitzky, *J. Lumin.* **52**, 201 (1992).
- ¹⁷R. Zimmermann, E. Runge, and F. Grosse, in *Proceedings of the 23rd International Conference on the Physics of Semiconductors*, edited M. Scheffler and R. Zimmermann (World Scientific, Singapore, 1996), Vol. 3, p. 1935.
- ¹⁸J. Puls, H.-J. Wünsche, and F. Henneberger, *Chem. Phys.* **210**, 235 (1996).
- ¹⁹J. Puls, V. V. Rossin, F. Henneberger, and R. Zimmermann, *Phys. Rev. B* **54**, 4974 (1996).
- ²⁰P. Peyla, R. Romestain, Y. Merle d'Aubigné, G. Fishman, A. Wasiela, and H. Mariette, *Phys. Rev. B* **52**, 12 026 (1995).
- ²¹A. Siarkos, E. Runge, and R. Zimmermann (unpublished).
- ²²G. L. Bir and G. E. Pikus, *Symmetry and Strain-Induced Effects in Semiconductors* (Wiley, New York, 1974).
- ²³R. Cingolani, P. Prete, D. Creco, P. V. Giugno, M. Lomascolo, R. Rinaldi, L. Calgagnile, L. Vanzetti, L. Sorba, and A. Franciosi, *Phys. Rev. B* **51**, 5176 (1995).
- ²⁴H. J. Lozykowski and V. K. Shastri, *J. Appl. Phys.* **69**, 3235 (1991).
- ²⁵H. W. Hölscher, A. Nöthe, and Ch. Uihlein, *Phys. Rev. B* **31**, 2379 (1985).
- ²⁶V. V. Rossin, F. Henneberger, and J. Puls, *Phys. Rev. B* **53**, 16 444 (1996).
- ²⁷D. A. Broido and L. J. Sham, *Phys. Rev. B* **34**, 3917 (1986); R. Winkler, *ibid.* **51**, 14 395 (1995).
- ²⁸J. Puls, F. Henneberger, M. Rabe, and A. Siarkos, *J. Cryst. Growth* **184/185**, 787 (1998).
- ²⁹G. E. W. Bauer and T. Ando, *Phys. Rev. B* **38**, 6015 (1988).
- ³⁰S. Rudin, T. L. Reinicke, and B. Segall, *Phys. Rev. B* **42**, 11 218 (1996); N. T. Pelekanos, J. Ding, M. Hagerott, A. V. Nurmikko, H. Luo, N. Samarth, and J. Furdyna, *Phys. Rev. B* **45**, 6037 (1992).
- ³¹I. Malikova, W. Krystek, F. H. Pollack, N. Dai, A. Cavus, and C. Tamargo, *Phys. Rev. B* **54**, 1819 (1996).
- ³²T. Miyami, F. P. Logue, J. F. Donegan, J. Hegarty, H. Okuyama, A. Ishibashi, and Y. Mori, *Appl. Phys. Lett.* **66**, 180 (1995).
- ³³K. Shahzad, J. Petrucello, J. M. Gines, and C. Ponzoni, *Appl. Phys. Lett.* **67**, 659 (1995).
- ³⁴E. Runge, A. Schülzgen, F. Henneberger, and R. Zimmermann, *Phys. Status Solidi B* **188**, 547 (1995).
- ³⁵M. Lowisch, J. Puls, and F. Henneberger (unpublished).